J. Fluid Mech. (1972), *vol.* 54, *part* 1, *pp.* 93–112
Printed in Great Britain

The stability of Poiseuille flow in a pipe of circular cross-section

By HAROLD SALWEN
Stevens Institute of Technology, Hoboken, New Jersey
AND CHESTER E. GROSCH
Pratt Institute, Brooklyn, New York

(Received 8 July 1971 and in revised form 6 March 1972)

The stability of Poiseuille flow in a pipe of circular cross-section to azimuthally varying as well as axisymmetric disturbances has been studied. The perturbation velocity and pressure were expanded in a complete set of orthonormal functions which satisfy the boundary conditions. Truncating the expansion yielded a matrix differential equation for the time dependence of the expansion coefficients. The stability characteristics were determined from the eigenvalues of the matrix, which were calculated numerically. Calculations were carried out for the azimuthal wavenumbers $n = 0, \ldots, 5$, axial wavenumbers α between 0·1 and 10·0 and $\alpha R \leqslant 50\,000$, R being the Reynolds number. Our results show that pipe flow is stable to infinitesimal disturbances for all values of α, R and n in these ranges.

1. Introduction

The stability of Poiseuille flow in a pipe of circular cross-section has been of continuing interest since Reynolds' classic experiments. Beginning with Rayleigh's (1892) paper, there have been a number of theoretical investigations of the stability of this flow. Rayleigh studied the inviscid stability of Poiseuille flow and concluded that the flow was stable to infinitesimal disturbances. He conjectured that the flow might be stable to infinitesimal disturbances but unstable to finite disturbances, or that the inviscid theory might be completely inapplicable to this problem.

A number of authors, including Sexl (1927), Synge (1938), Pretsch (1941), Pekeris (1948), Tatsumi (1952), Corcos & Sellars (1959), Schensted (1960), Gill (1965) and Davey & Drazin (1969), have studied theoretically the stability of Poiseuille flow to axisymmetric disturbances for all values of the Reynolds number.

Following Reynolds' experiments, there have been a number of other experimental studies of the stability of Poiseuille flow (see Dryden (1959) for a discussion of some of these experiments). These have all shown that, by excluding disturbances, the onset of instability can be delayed to very high Reynolds numbers. This appears to support the idea that the observed instabilities are due to finite amplitude effects.

On the other hand, it might be expected, by analogy with plane Poiseuille flow, that the axisymmetric disturbances would be stable. (In plane Poiseuille flow no growing disturbances with the same symmetry as the base flow have been found. The growing disturbance has opposite symmetry to the base flow.) It is therefore necessary, before concluding that Poiseuille flow is stable to infinitesimal disturbances, to examine the stability of this flow to non-axisymmetric disturbances. Recent experiments by Lessen, Fox, Bhat & Liu (1964) and Fox, Lessen & Bhat (1968) on the growth of non-axisymmetric disturbances confirm the importance of studying such disturbances theoretically.

In the work reported here we have studied the stability of Poiseuille flow to disturbances with an azimuthal variation of the form $e^{in\theta}$ for $n = 0, \ldots, 5$. A preliminary report (Salwen & Grosch 1968) of this work was presented at the 1967 meeting of the Division of Fluid Dynamics of the A.P.S. Lessen, Sadler & Liu (1968) have independently studied the $n = 1$ modes by a different numerical method; there have also been recent analytic studies by Burridge & Drazin (1969) and Graebel (1970).

The method which we have used consists of expanding the perturbation velocity and pressure in a complete set of orthonormal functions which satisfy the boundary conditions. Truncating the expansion yields a matrix differential equation for the time dependence of the expansion coefficients. The stability characteristics are determined from the eigenvalues of the matrix, which are calculated numerically.

In §2 we formulate the solution in terms of orthogonal functions and in §3 we derive the expansion functions. Section 4 contains a discussion of the accuracy of the calculations. The results for the $n = 0$ modes and comparisons with the work of previous investigators of these axisymmetric modes are given in §5.1. In §5.2 we give our results for $n = 1, \ldots, 5$ and compare them with those of Lessen *et al.* (1968), Burridge & Drazin (1969) and Graebel (1970). Section 6 is a brief statement of our conclusions.

2. Formulation

We wish to study the stability of Poiseuille flow in a circular pipe. That is, we consider the base flow to be the laminar flow of an incompressible fluid in a circular pipe under the influence of a constant pressure gradient. The velocity profile is then the familiar parabolic profile with maximum speed W_0 on the centre-line. In the remainder of this paper, dimensionless variables will be used: the length scale is r_0, the radius of the pipe; the velocity scale is W_0; the time scale is r_0/W_0 and the pressure scale is ρW_0^2, where ρ is the density. The Reynolds number of the flow is $R = W_0 r_0/\nu$, where ν is the kinematic viscosity. Cylindrical co-ordinates (r, θ, z) will be used, with $r = 0$ at the centre-line of the pipe and z increasing in the downstream direction. The base flow is, in this co-ordinate system,

$$\mathbf{V} = W(r)\hat{\mathbf{k}} = (1-r^2)\hat{\mathbf{k}}. \tag{1}$$

Consider a small disturbance to the flow. The velocity is then $\mathbf{V}+\mathbf{v}$ and the pressure is $P+p$, where $\mathbf{V}$ and P are the velocity and pressure of the base flow

and $\mathbf{v}$ and p are the velocity and pressure arising from the disturbance. By substituting into the Navier–Stokes equations, noting that $\mathbf{V}$ and P already give a solution and retaining only terms which are linear in $\mathbf{v}$, we find that $\mathbf{v}$ and p satisfy

$$\nabla . \mathbf{v} = 0, \tag{2}$$

$$\frac{\partial \mathbf{v}}{\partial t} + \nabla(\mathbf{V}.\mathbf{v}) - \mathbf{V} \times (\nabla \times \mathbf{v}) - \mathbf{v} \times (\nabla \times \mathbf{V}) = -\frac{1}{R}\nabla \times (\nabla \times \mathbf{v}) - \nabla p. \tag{3}$$

We shall consider the 'timewise' problem, i.e. the growth or decay of disturbances as a function of time. Since the base flow and (2) and (3) are invariant with respect to translations in the z direction and rotations about the z axis, the normal modes will be of the form

$$p = \Pi_0(r,t)\, e^{i(n\theta+\alpha z)}, \tag{4}$$

$$\mathbf{v} = [u_0(r,t)\,\hat{\mathbf{e}}_r + v_0(r,t)\,\hat{\mathbf{e}}_\theta + w_0(r,t)\,\hat{\mathbf{k}}]\, e^{i(n\theta+\alpha z)}, \tag{5}$$

where α is an arbitrary real number and n is an integer. Finally, the boundary conditions are that the velocity is zero on the walls of the pipe, i.e.

$$\mathbf{v} = 0 \quad \text{for} \quad r = 1, \tag{6}$$

and that $\mathbf{v}$ and p are bounded.

We now choose a set of expansion functions $\mathbf{v}_l$ and p_l, which are the eigensolutions (with eigenvalue λ_l) of

$$\nabla . \mathbf{v}_l = 0, \tag{7}$$

$$\lambda_l \mathbf{v}_l = -(1/R)\nabla \times (\nabla \times \mathbf{v}_l) - \nabla p_l \tag{8}$$

(equation (3) with $\mathbf{V} = 0$ and λ_l replacing $\partial/\partial t$), having the same θ and z dependence and satisfying the same boundary conditions as the disturbances. It is easily shown that

$$(\lambda_k^* - \lambda_l)\langle \mathbf{v}_k, \mathbf{v}_l \rangle = \iiint [\lambda_k^* \mathbf{v}_k^* . \mathbf{v}_l - \mathbf{v}_k^* . \lambda_l \mathbf{v}_l]\, d\tau = 0, \tag{9}$$

where the inner product $\langle \mathbf{f}, \mathbf{g} \rangle$ is defined by

$$\langle \mathbf{f}, \mathbf{g} \rangle = \iiint \mathbf{f}^* . \mathbf{g}\, d\tau, \tag{10}$$

the star indicates the complex conjugate, and the integration is over a volume within the pipe bounded by two planes perpendicular to the axis of the pipe and one wavelength ($= 2\pi/\alpha$) apart. Then, with appropriate normalization,

$$\langle \mathbf{v}_k, \mathbf{v}_l \rangle = \delta_{kl} \tag{11}$$

and the eigenvalues are real.

Assuming that the expansion functions are known (they will be derived in detail in §3 below), we expand the disturbance velocity $\mathbf{v}$ in a series in the functions $\mathbf{v}_k$:

$$\mathbf{v} = \sum_{k=1}^{\infty} a_k(t)\, \mathbf{v}_k, \tag{12}$$

so that

$$a_k = \langle \mathbf{v}_k, \mathbf{v} \rangle. \tag{13}$$

Each term in this expansion satisfies the continuity equation (2) and the boundary conditions.†

From (13) we have

$$\begin{aligned} da_k/dt &= \langle \mathbf{v}_k, \partial \mathbf{v}/\partial t \rangle \\ &= \langle \mathbf{v}_k, -\nabla(\mathbf{V}.\mathbf{v}) + \mathbf{V}\times(\nabla\times\mathbf{v}) + \mathbf{v}\times(\nabla\times\mathbf{V}) - (1/R)\nabla\times(\nabla\times\mathbf{v}) - \nabla p\rangle \\ &= \langle \nabla\times(\mathbf{v}_k\times\mathbf{V}) - \mathbf{v}_k\times(\nabla\times\mathbf{V}), \mathbf{v}\rangle + \lambda_k\langle \mathbf{v}_k, \mathbf{v}\rangle \\ &= \sum_{l=1}^{\infty} G_{kl}a_l + \lambda_k a_k, \end{aligned} \tag{14}$$

where

$$G_{kl} = \langle \nabla\times(\mathbf{v}_k\times\mathbf{V}) - \mathbf{v}_k\times(\nabla\times\mathbf{V}), \mathbf{v}_l\rangle. \tag{15}$$

Equation (14) determines the time dependence of the disturbances. We now turn to the solution of the eigenvalue equations (7) and (8) in order to determine the coefficients λ_k and G_{kl}.

3. Expansion functions

The expansion functions are the solutions of (7) and (8). Dropping the subscripts for convenience, we define $w(r,\theta)$ and $\mathbf{v}_\perp(r,\theta)$ by

$$w(r,\theta) = \hat{\mathbf{k}}.\mathbf{v}\,e^{-i\alpha z}, \tag{16}$$

$$\mathbf{v}_\perp(r,\theta) = -\hat{\mathbf{k}}\times(\hat{\mathbf{k}}\times\mathbf{v})\,e^{-i\alpha z}, \tag{17}$$

so that

$$\mathbf{v} = (\mathbf{v}_\perp + w\hat{\mathbf{k}})\,e^{i\alpha z}. \tag{18}$$

We similarly define $p_0(r,\theta)$ by

$$p_0(r,\theta) = p\,e^{-i\alpha z}. \tag{19}$$

Then (7) and (8) become

$$\nabla.\mathbf{v}_\perp + i\alpha w = 0, \tag{20}$$

$$(\nabla^2 - \alpha^2 - \lambda R)\,\mathbf{v}_\perp = R\nabla p_0, \tag{21}$$

$$(\nabla^2 - \alpha^2 - \lambda R)\,w = i\alpha R p_0. \tag{22}$$

If we define scalar and vector potentials $\Phi(r,\theta)$ and $\boldsymbol{\Psi}(r,\theta)$ by

$$\Phi = (-1/\lambda)\,p_0, \tag{23}$$

$$\boldsymbol{\Psi} = (-i/\alpha)\,(\mathbf{v}_\perp - \nabla\Phi), \tag{24}$$

these potentials must satisfy

$$(\nabla^2 - \alpha^2)\,\Phi = (-1/\lambda R)\,(\nabla^2 - \alpha^2 - \lambda R)\,(\nabla.\mathbf{v}_\perp + i\alpha w) = 0, \tag{25}$$

and

$$(\nabla^2 - \alpha^2 - \lambda R)\,\boldsymbol{\Psi} = (-i/\alpha)\,[(\nabla^2 - \alpha^2 - \lambda R)\,\mathbf{v}_\perp - R\nabla p_0] = 0. \tag{26}$$

In terms of Φ and $\boldsymbol{\Psi}$ we have

$$\mathbf{v}_\perp = \nabla\Phi + i\alpha\boldsymbol{\Psi}, \tag{27}$$

$$w = (i/\alpha)\,\nabla.\mathbf{v}_\perp = i\alpha\Phi - \nabla.\boldsymbol{\Psi}, \tag{28}$$

$$p_0 = -\lambda\Phi. \tag{29}$$

† Note that p will, in general, not be equal to $\Sigma a_k p_k$. In fact, $\nabla^2 p_k = 0$ for all k, and $\nabla^2 p \neq 0$. These considerations do not affect the validity of the velocity expansion because, since $\langle \mathbf{v}_k, \nabla p\rangle = 0$, the pressure term drops out of equation (14).

It is apparent that, with $\mathbf{v}_\perp$, w and p_0 given by (27), (28) and (29) and the potentials obeying (25) and (26), the eigenvalue equations (20), (21) and (22) will be satisfied.

In order for p and $\mathbf{v}$ to satisfy (4) and (5) we must have

$$\Phi = \phi(r)\, e^{in\theta}, \tag{30}$$

$$\Psi = [\psi_r(r)\,\hat{\mathbf{e}}_r + \psi_\theta(r)\,\hat{\mathbf{e}}_\theta]\, e^{in\theta}. \tag{31}$$

If (31) is substituted into (26) a pair of coupled equations for ψ_r and ψ_θ will result. These can be decoupled by defining

$$\psi_\pm = \tfrac{1}{2}(\psi_r \pm i\psi_\theta). \tag{32}$$

Equations (25) and (26) then yield

$$(L_n - \alpha^2)\,\phi = 0, \tag{33}$$

$$(L_{n\pm1} - \alpha^2 - \lambda R)\,\psi_\pm = 0, \tag{34}$$

where

$$L_n \equiv \frac{1}{r}\frac{d}{dr}\left(r\frac{d}{dr}\right) - \frac{n^2}{r^2}. \tag{35}$$

The boundary condition (6) then becomes

$$\left[\frac{d}{dr}(r^{\mp n}\phi)\right]_{r=1} + 2i\alpha\psi_\pm(1) = 0, \tag{36}$$

$$\left[\frac{d}{dr}(r^{n+1}\psi_+)\right]_{r=1} + \left[\frac{d}{dr}(r^{-n+1}\psi_-)\right]_{r=1} - i\alpha\phi(1) = 0. \tag{37}$$

The solutions of (33) and (34) are

$$\phi = C_0 I_n(\alpha r) = C_0 J_n(i\alpha r), \tag{38}$$

$$\psi_\pm = C_\pm J_{n\pm1}(\beta r), \tag{39}$$

where $J_{n\pm1}$ are Bessel functions and I_n a modified Bessel function, both of the first kind, and

$$\beta = [-\lambda R - \alpha^2]^{\frac{1}{2}}. \tag{40}$$

When the solutions (38) and (39) are substituted into the boundary conditions (36) and (37) we obtain homogeneous linear equations for the constants C_0, C_+ and C_-. The secular determinant yields the eigenvalue equation

$$\beta\left[\frac{J_n'(\beta)}{J_n(\beta)}\right]\left[\frac{J_n'(\beta)}{\beta J_n(\beta)} + \frac{I_n'(\alpha)}{\alpha I_n(\alpha)}\right] - \frac{n^2(\alpha^2+\beta^2)}{\alpha^2\beta^2} = 0. \tag{41}$$

Apart from the trivial root $\beta = i\alpha$ (which leads to $\phi = 0$, $\psi_\pm = 0$), all the eigenvalues of β are real and can be found by an appropriate iteration procedure.

Once the eigenvalues

$$\lambda_k = (-1/R)\,(\alpha^2 + \beta_k^2) \tag{42}$$

have been obtained, the calculation of the potentials and the expansion functions is straightforward.

4. Numerical calculations

4.1. *Method of calculation*

We now assume that the expansion for the disturbance velocity $\mathbf{v}$ can be truncated after N terms, i.e. in (12) we put

$$\mathbf{v} \approx \sum_{k=1}^{N} a_k(t)\,\mathbf{v}_k. \tag{43}$$

Then the a_k, $k = 1, 2, \ldots, N$, are a solution of (14):

$$\frac{da_k}{dt} = \lambda_k a_k + \sum_{l=1}^{N} G_{kl} a_l. \tag{44}$$

In matrix notation, we have

$$d\mathbf{A}/dt = \mathbf{F}\mathbf{A}, \tag{45}$$

where $\mathbf{A}$ is the column vector of the a_k and $\mathbf{F}$ is the $(N \times N)$ matrix defined by

$$\mathbf{F}_{kl} = \mathbf{G}_{kl} + \lambda_k \delta_{kl}. \tag{46}$$

Equation (45) possesses a complete set of solutions of the form

$$\mathbf{A}_k = \mathbf{Q}_k e^{\sigma_k t}, \tag{47}$$

σ_k being an eigenvalue of $\mathbf{F}$. If σ_k is a simple eigenvalue, then $\mathbf{Q}_k$ is a constant, but if σ_k is a multiple eigenvalue, of multiplicity K, say, then $\mathbf{Q}_k$ is a polynomial of degree $K-1$. The flow will be stable only if all of the eigenvalues of $\mathbf{F}$ have a negative real part. If there is any eigenvalue with a positive real part then the flow will be unstable with an exponential growth. It is also possible for the flow to be unstable with an algebraic growth in time. This will occur if there is a multiple eigenvalue with the real part identically zero. Thus the stability characteristics of the flow are completely determined by the eigenvalues of $\mathbf{F}$.

The eigenvalues of $\mathbf{F}$ were calculated numerically using the QR algorithm (Parlett 1967). The calculation of all of the eigenvalues of $\mathbf{F}$, when $\mathbf{F}$ is 30×30, takes about 2 min on an IBM 360/40 and the calculation time is proportional to N^3.

The results will be given in this paper in terms of the complex wave speed of the disturbance, c_k, instead of σ_k. These are related by

$$\sigma_k = -i\alpha c_k^*. \tag{48}$$

The flow will thus be unstable if, for some k,

$$\mathrm{Im}\,(c_k) < 0. \tag{49}$$

The eigenvalues are numbered in the order of increasing imaginary part of c_k. The order is taken to be that at small R.

4.2. *Accuracy*

The method of this calculation is essentially the same as that used in our calculation of plane Poiseuille flow (Grosch & Salwen 1968). In that case exact agreement was obtained with the four-significant-figure eigenvalues obtained by

	$N = 2$		$N = 30$	
	Re (c)	Im (c)	Re (c)	Im (c)
$\alpha = 1, R = 10$	0·463727	1·38289	0·463831	1·39190
	0·765128	2·79932	0·764578	2·80969
$\alpha = 10^{-4}, R = 10^5$	0·647287	1·44481	0·647740	1·44321
	0·815926	2·66085	0·815293	2·66518

TABLE 1. Two examples of convergence for $\alpha R = 10, n = 1$. The first two eigenvalues are listed for $N = 2$ and $N = 30$ and two different values of (α, R)

Thomas (1953) by an altogether different numerical method. Comparisons between our present results and other work on pipe flow are given in §5 of this paper.

It is unlikely that significant errors have been made in the solution of the truncated problem (equation (45)). The most likely sources of error in this calculation are our Bessel function routine (used to evaluate the eigenvalues λ_k of the expansion functions as well as in explicit formulae for the F_{kl}), our iterative routine for the λ_k and our matrix eigenvalue routine. Our Bessel function routine has been checked against published tables and is accurate to about one part in 10^7. The iteration for the eigenvalues of the expansion function was continued until the relative error was less than 2×10^{-8}. The QR algorithm used to calculate matrix eigenvalues is renowned for its stability. The particular program we used is a modification of Parlett's (1967) routine and contains (as an internal check) a comparison of the trace with the sum of the eigenvalues. Under most circumstances no individual root contains an error much larger than that in the eigenvalue sum. By these criteria we estimate that the eigenvalues of $\mathbf{F}$ have been calculated to six significant figures.

The remaining source of error is truncation (the fact that we have used a finite matrix instead of an infinite one). This clearly can produce significant errors. The best way to study the effect of truncation on accuracy is to compare the eigenvalues of the same problem for different values of N, that is, the convergence of the calculated eigenvalues as N increases. This is discussed in the following section.

4.3. *Convergence*

As would be expected from our choice of expansion functions, the convergence of this expansion is extremely rapid for sufficiently small values of αR (less than or about equal to 20). Two examples of this convergence are given in table 1. It is clear that in these cases ($\alpha R = 10$ for both) the eigenvalues calculated from a two-term expansion have already converged to better than 1 %.

For larger values of αR, convergence is slower and it is necessary to use larger matrices. If N is too small, the c's vary wildly with small changes in N; it is even possible to find *spurious* instabilities (negative Im (c)). Once N is large enough the first one or two c's are found to have converged, or almost so; other low-lying modes have also nearly converged but are scattered among a number of

	$N = 30$		$N = 50$		$N = 70$	
	Re (c)	Im (c)	Re (c)	Im (c)	Re (c)	Im (c)
1	0·951583	0·022690	0·951583	0·022686	0·951583	0·022687
2	0·251741	0·027474	0·276663	0·037047	0·276712	0·037022
3	0·410591	0 031003	0·977105	0·048455	0·977104	0·048455
4	0·316216	0·036548	0·920732	0·048917	0·920732	0·048917
5	0·502885	0·040384	0·890843	0·075781	0·890842	0·075782
6	0·583306	0·042203	0·950690	0·079258	0·950690	0·079258
7	0·660988	0·047531	0·146491	0·080631	0·146507	0·080593
8	0·977104	0·048454	0·861460	0·102775	0·861464	0·102767
9	0·921227	0·048791	0·923686	0·109138	0·923686	0·109138
10	0·728593	0·051039	0·391871	0·127081	0·391506	0·127305
11	0·790592	0·055377	0·831822	0·130745	0·831828	0·130781
12	0·844352	0·059139	0·896402	0·138606	0·896401	0·138608
13	0·890355	0·062299	0·254985	0·141122	0·254962	0·141111
14	0·132331	0·075175	0·804990	0·158852	0·804912	0·158747
15	0·950596	0·079335	0·868925	0·167659	0·868922	0·167663

TABLE 2. The first fifteen eigenvalues, arranged in order of increasing imaginary part of c, for three different sizes of the matrix; $N = 30$, 50 and 70. For all N, $\alpha = 1{\cdot}0$, $R = 10^4$ and $n = 1$.

spurious modes. With increasing N, these spurious modes vary rapidly and eventually disappear until finally an appreciable number (depending on α, R and n) of eigenvalues converge.

A typical example of this behaviour at larger αR is given in table 2. In this example, $\alpha = 1{\cdot}0$, $R = 10^4$ and $n = 1$. The first fifteen eigenvalues, arranged in order of increasing imaginary part of c, are tabulated for three different sizes of the matrix ($N = 30$, 50 and 70). We have also carried out calculations with the same values of α, R and n for $N = 20$, 40, 60 and 80. From an examination of the results for $N = 60$, 70 and 80, it is apparent that the 15 eigenvalues shown have converged to at least four significant figures for $N = 70$.

With $N = 20$ (results not shown) the accuracy was so poor that 5 of the c's had *negative* imaginary parts, and it was not possible to identify any of the eigenvalues with members of the converged set. Examining table 1 shows that with $N = 30$ the first eigenvalue has converged to 5 significant figures while the second is within 10% of its converged value. With $N = 30$, eigenvalues 3–7 and 10–12 are spurious eigenvalues and have no counterparts in the final converged set. The eigenvalues which are numbers 3 and 4 for $N = 70$ are numbers 8 and 9 with $N = 30$, and those which are 5, 6 and 7 at $N = 70$ are 13, 15 and 14, respectively, at $N = 30$. Eigenvalues 8–15 at $N = 70$ have no counterparts at $N = 30$.

It is clear, from the results shown in table 1, that the slow modes (numbers 2, 7, 10 and 13 at $N = 70$) converge somewhat slower than the fast modes. We have found that this is generally true for large αR.

Finally, the order of modes at high R, as given in this table, is not the same as the order of the modes at low R which we use to number the modes. This is due, as will be seen below, to the cross-overs of the eigenvalues as R varies.

The least stable (lowest) mode at small R is also the least stable mode at sufficiently large R but for the other modes there can be considerable change in the order from small to large R. Here, at $N = 70$, mode 1 is the first mode in the table but mode 2 is seventh, mode 3 is third and mode 4 is second.

It should be pointed out that when there are two almost degenerate eigenvalues (both real and imaginary parts) the error in calculating them may be considerably larger than that of the other eigenvalues. This happens because both truncation errors and small errors in calculating off-diagonal matrix elements normally influence the eigenvalues to second order but in the case of degeneracy may produce first-order effects.

5. Results

5.1. *Rotationally symmetric modes*

In figures 1 (*a*) and (*b*) we have plotted our results for the real and imaginary parts of the first six eigenvalues as functions of R for $\alpha = 1$ and $n = 0$ and shown the comparison with various asymptotic approximations. The modes are numbered according to the magnitude of $\mathrm{Im}\,(c)$ at low Reynolds number. With this ordering, the odd modes are torsional and the even modes are meridional.† The solid lines on these figures are our numerical results; the dashed lines are obtained from asymptotic calculations.

In the region $\alpha R \lesssim 500$, the dashed curves for the meridional modes (2, 4 and 6) have been calculated from an approximation due to Pekeris.‡ The dashed curves for the torsional modes (1, 3 and 5) were calculated by using an extension of Pekeris's method. The agreement with our results at low R is excellent. As $R \to 0$, the difference between dashed and solid curves is not visible.

Pekeris has also developed a second asymptotic approximation,§ valid for those modes for which $|c| \approx 1$ when $\alpha R \to \infty$ with α not too large. Though this approximation was derived for meridional modes, it is easily seen from an extension of Pekeris's method that to each meridional eigenvalue calculated by this method there corresponds a torsional eigenvalue approximately equal to it. The high R curves labelled P in figure 1 are calculated by this asymptotic method ($P1$ is the least stable of these modes and $P2$ is the next one). The points on these curves correspond to *both* torsional and meridional eigenvalues since our calculation (in agreement with the comment above) gives almost equal (to 0·1 %) values for these pairs of eigenvalues. Again it may be seen that our results are in such good agreement with those of Pekeris that the curves merge at high R. These modes have both $[1 - \mathrm{Re}\,(c)]$ and $\mathrm{Im}\,(c)$ proportional to $(\alpha R)^{-\frac{1}{3}}$. We call these the 'fast' modes since the wave speed $\mathrm{Re}\,(c)$ approaches unity as $\alpha R \to \infty$.

In addition to the 'fast' modes discussed in the preceding paragraph there are, at high R, various normal modes with $\mathrm{Re}\,(c)$ ranging from 0 to about $\frac{2}{3}$.

† For torsional modes $u_0 = w_0 = 0$ and for meridional modes $v_0 = 0$, see Pekeris (1948, p. 287).

‡ See Pekeris (1948, equation (37)).

§ See Pekeris (1948, equation (44)).

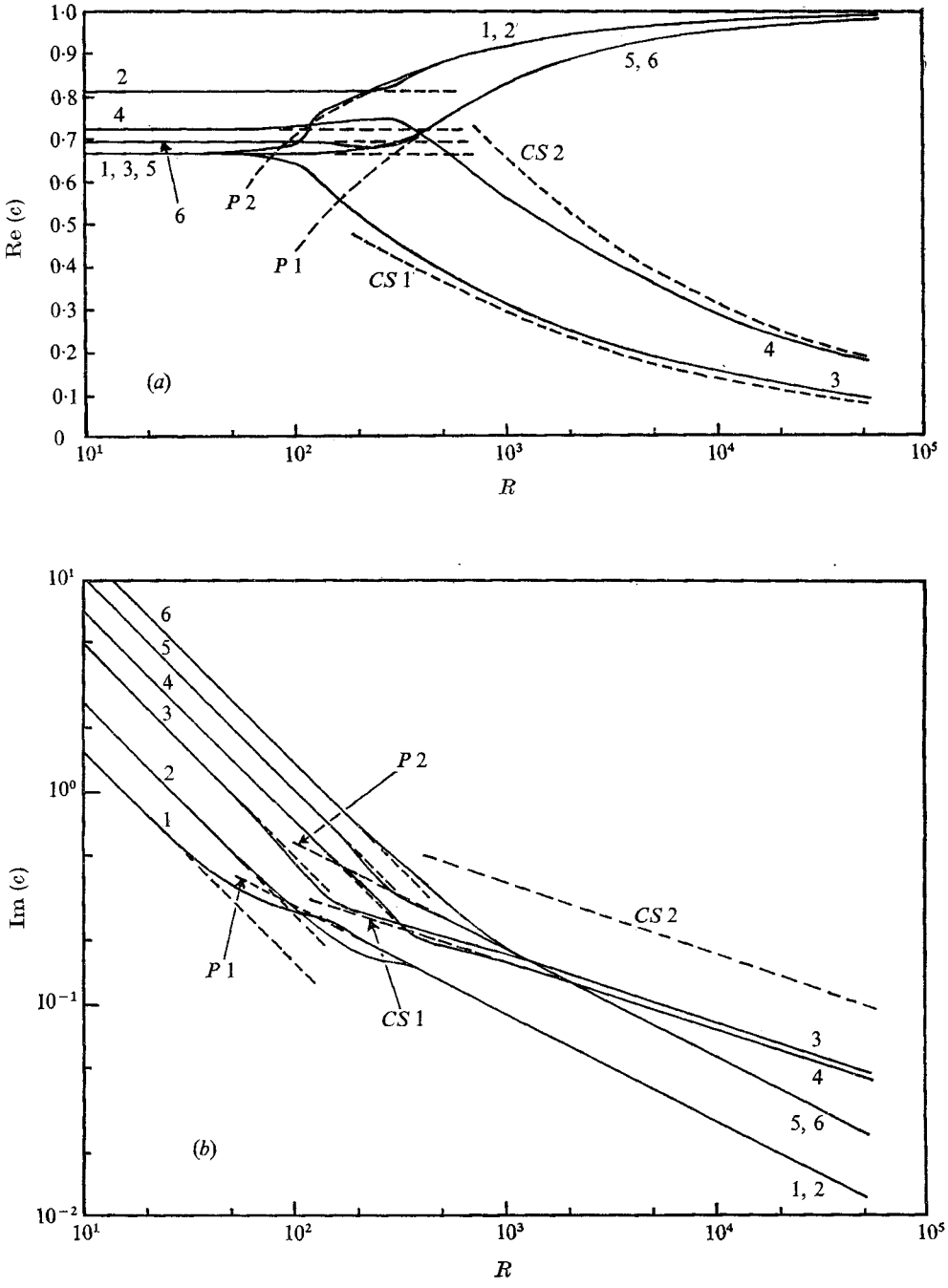

FIGURE 1. Variation of (*a*) the real part of the first six eigenvalues (i.e. the wave speed) and (*b*) the imaginary part with the Reynolds number for the axisymmetric ($n = 0$) mode. The axial wavenumber $\alpha = 1{\cdot}0$. Solid curves are the results of our numerical calculations and the dashed curves are various asymptotic approximations discussed in the text.

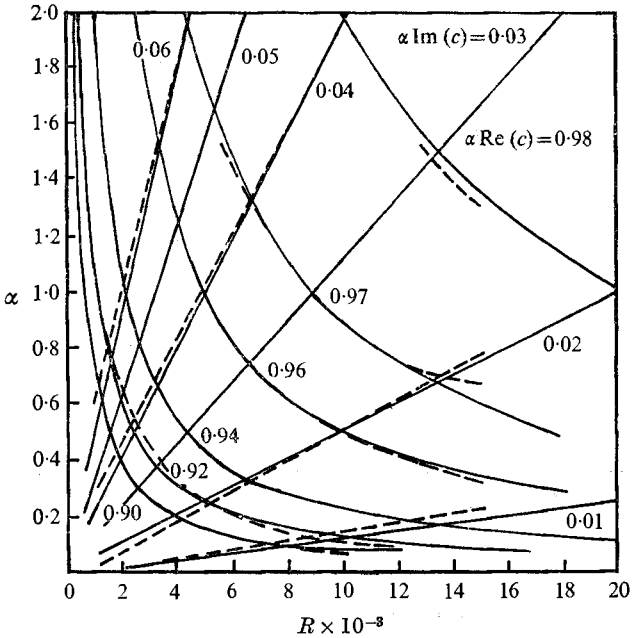

FIGURE 2. Curves of constant Re (αc) and Im (αc) for the least stable axisymmetric mode ($n = 0$) in the α, R plane. The solid lines are the results of our numerical calculation and the dashed curves are the results of a numerical calculation of Davey & Drazin (1969).

Corcos & Sellars (1959), in addition to reproducing Pekeris's $|c| \approx 1$ approximation, have developed two different asymptotic approximations which should be valid for meridional modes with $c \approx 0$. We call these the 'slow' modes. The curves *CS* in figure 1 are calculated by one of these approximations. Modes 3 and 4 are the least stable of the slow modes. *CS*1 and *CS*2 refer to the two least stable slow modes as calculated by Corcos & Sellars. As can be seen in figure 1(*a*), the real parts of modes 3 and 4 are approximately in agreement with *CS*1 and *CS*2, respectively. In figure 1(*b*) it can be seen that at high R the curve for *CS*1 merges with that of mode 4 and is approximately equal to that of mode 3, but, surprisingly, *CS*2 is considerably different. These slow modes have both Re (c) and Im (c) proportional to $(\alpha R)^{-\frac{1}{3}}$. It is clear that the functional dependence of our numerical results is the same as that of the analytic results of Corcos & Sellars.

We have carried out a number of calculations for other values of α and R. Figure 2 shows some of these results and a comparison with the results of a numerical calculation of Davey & Drazin (1969). This figure is a plot of the curves of constant Re (αc) and Im (αc) in the α, R plane for the least stable mode, with the results of Davey & Drazin (1969) (dashed curves) superposed upon the graph of our results (solid curves). As can be seen, the agreement is good.

5.2. *Azimuthally varying modes*

In addition to the azimuthally symmetric mode $n = 0$, we have studied the azimuthally varying modes, $n = 1$–5, for $0{\cdot}1 \leqslant \alpha \leqslant 10{\cdot}0$ and $\alpha R \leqslant 50000$. We

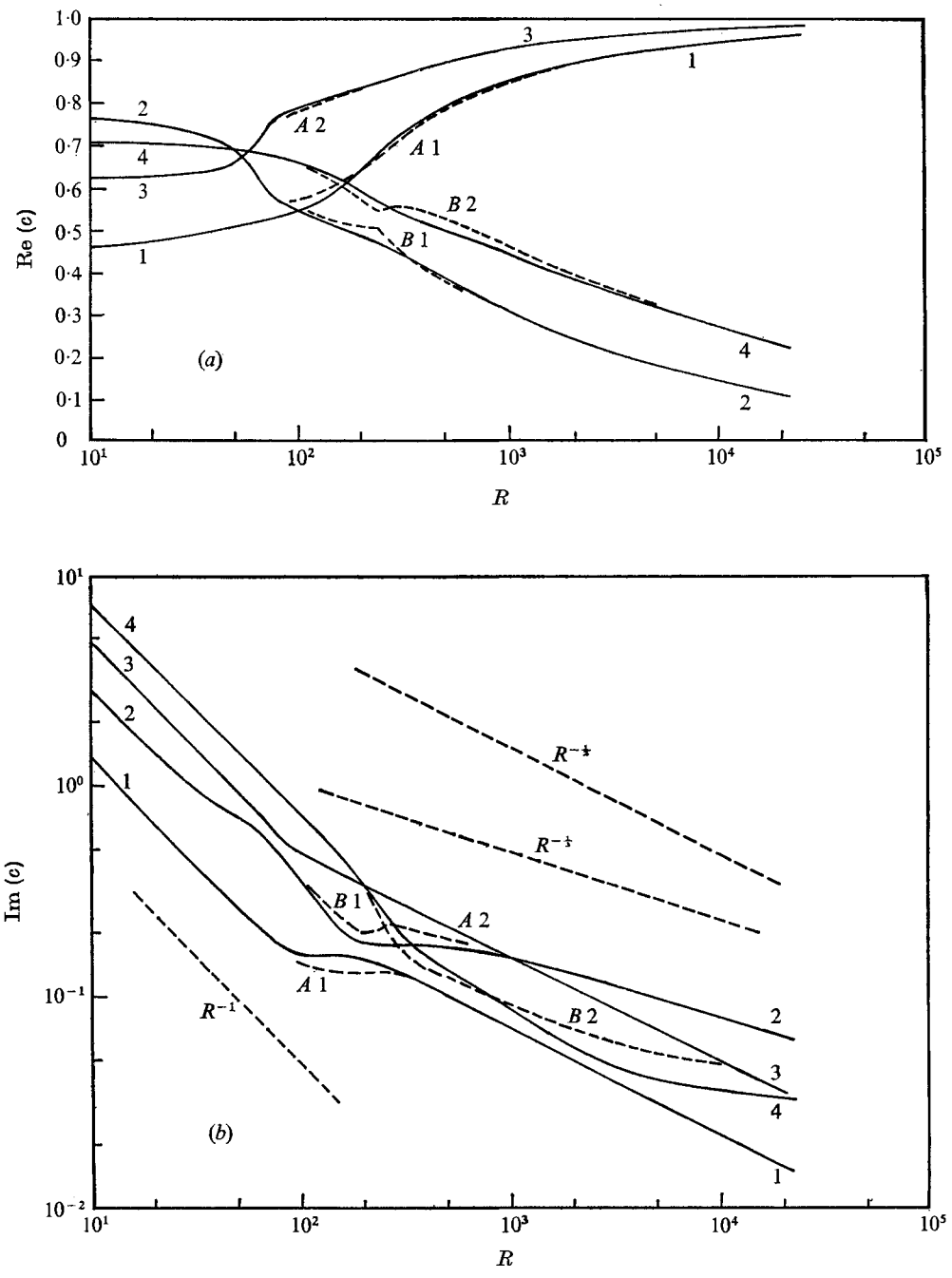

FIGURE 3. Variation of (*a*) the real part and (*b*) the imaginary part of the first four eigenvalues with Reynolds number for the first ($n = 1$) azimuthally varying mode. The axial wavenumber $\alpha = 1{\cdot}0$. Solid curves are the results of our numerical calculation and dashed curves the results of numerical calculations of Lessen, Sadler & Liu (1968). Dashed lines showing an R^{-1}, $R^{-\frac{1}{2}}$ and $R^{-\frac{1}{3}}$ variation are also shown.

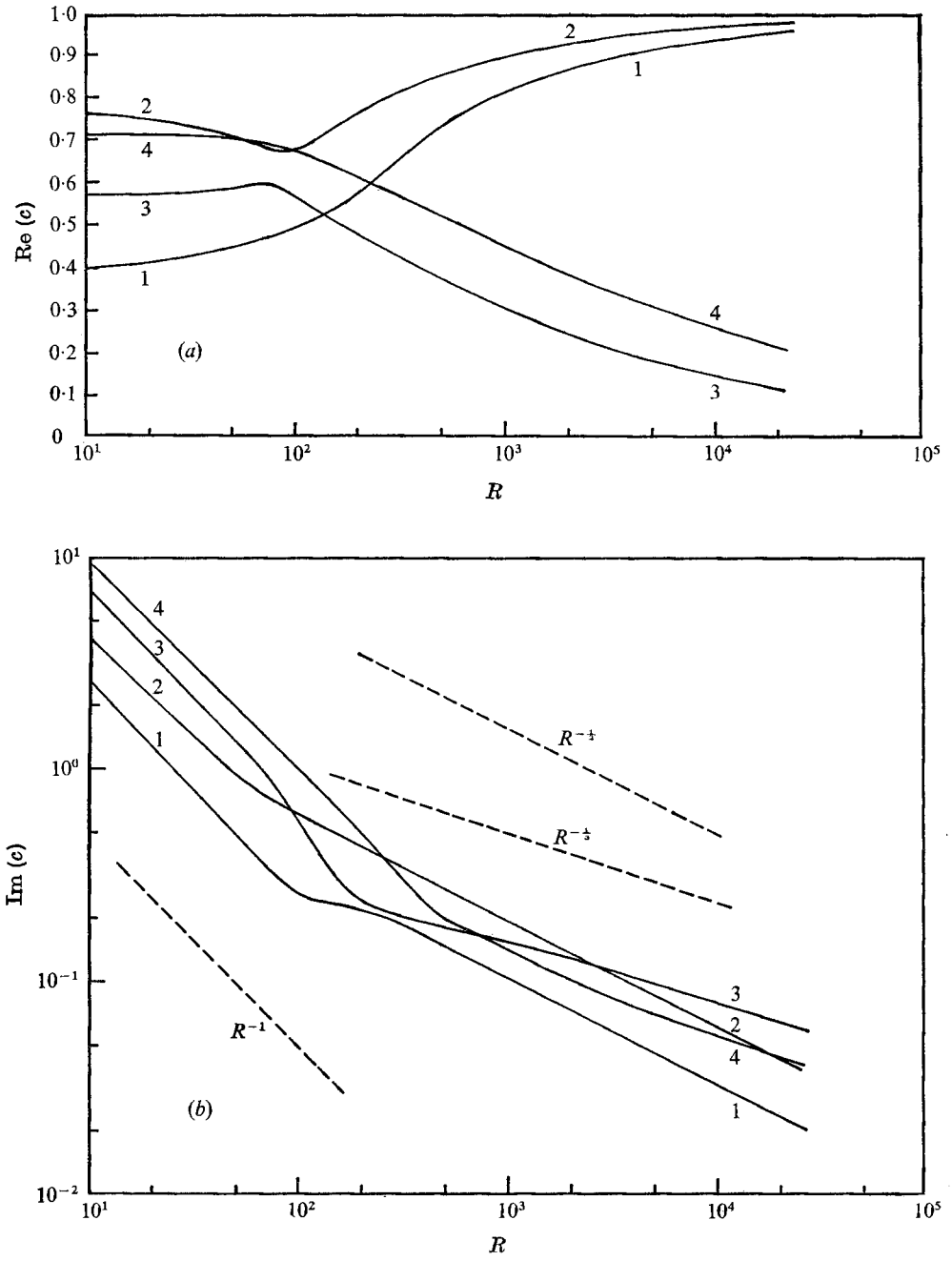

FIGURE 4. Variation of (*a*) the real part and (*b*) the imaginary part of the first four eigenvalues with Reynolds number for the second ($n = 2$) azimuthally varying mode. The axial wavenumber $\alpha = 1{\cdot}0$. The dashed lines show an R^{-1}, $R^{-\frac{1}{2}}$ and $R^{-\frac{1}{3}}$ variation.

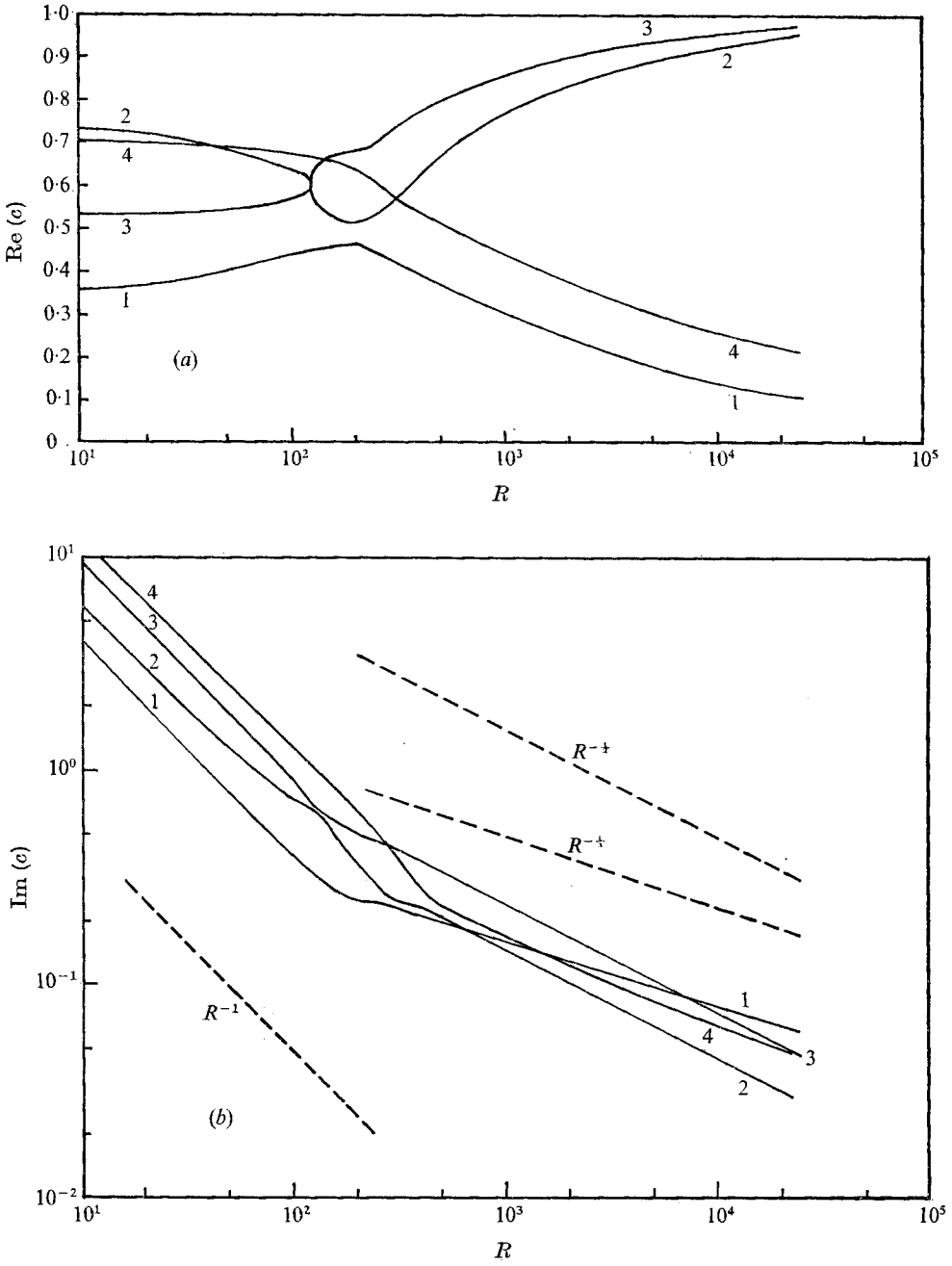

FIGURE 5. Variation of (*a*) the real part and (*b*) the imaginary part of the first four eigenvalues with Reynolds number for the third ($n = 3$) azimuthally varying mode. The axial wavenumber $\alpha = 1{\cdot}0$. The dashed lines show an R^{-1}, $R^{-\frac{1}{2}}$ and $R^{-\frac{1}{3}}$ variation.

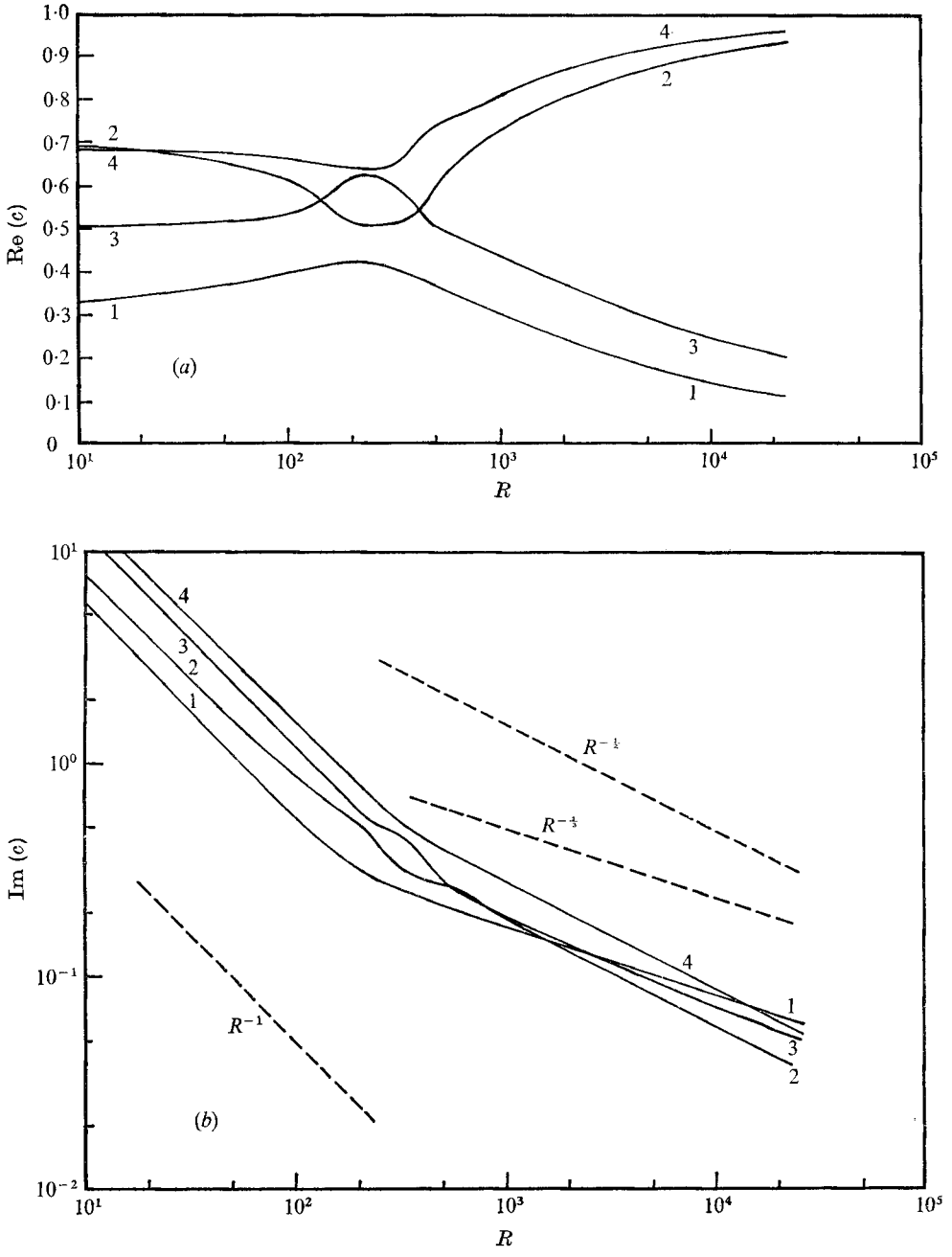

FIGURE 6. Variation of (*a*) the real part and (*b*) the imaginary part of the first four eigenvalues with Reynolds number for the fourth ($n = 4$) azimuthally varying mode. The axial wavenumber $\alpha = 1{\cdot}0$. The dashed lines show an R^{-1}, $R^{-\frac{1}{2}}$ and $R^{-\frac{1}{3}}$ variation.

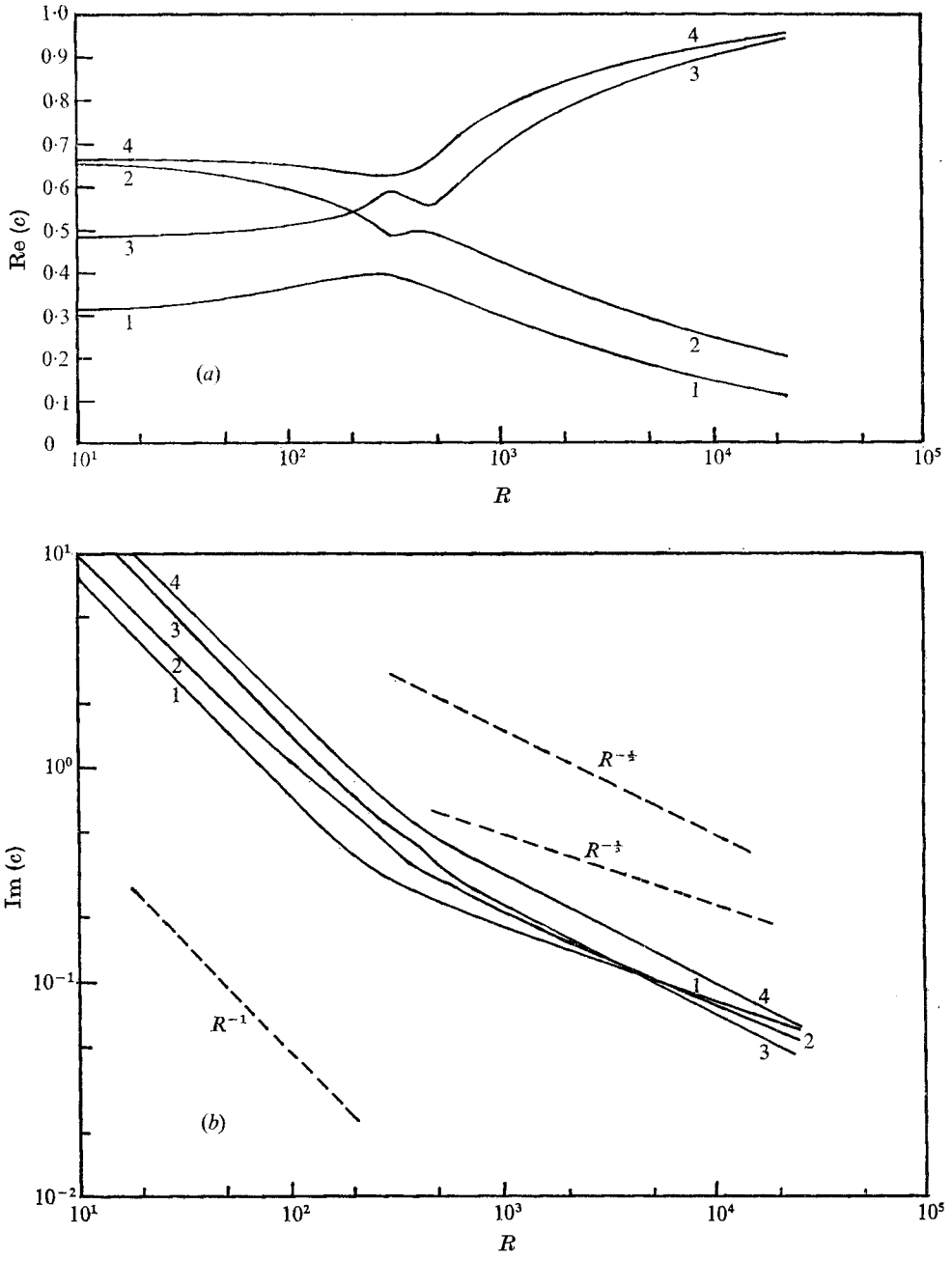

FIGURE 7. Variation of (*a*) the real part and (*b*) the imaginary part of the first four eigenvalues with Reynolds number for the fifth ($n = 5$) azimuthally varying mode. The axial wavenumber $\alpha = 1{\cdot}0$. The dashed lines show an R^{-1}, $R^{-\frac{1}{2}}$ and $R^{-\frac{1}{3}}$ variation.

have found in all cases considered that the flow is stable to infinitesimal disturbances.

Figures 3–7 show the real and imaginary parts of c for the four lowest modes for $\alpha = 1{\cdot}0$, $R \leqslant 20\,000$, and $n = 1$–5. Lessen *et al.* (1968)† have calculated c in the same range for $n = 1$ by numerical integration. Their results are compared with ours on figures 3(*a*) and (*b*). As can be seen from figure 3, there is fairly good agreement between our results and those of Lessen *et al.* except for R near 250, where our eigenvalue 2 and their corresponding eigenvalue $B1$ differ considerably. This is just the region where c_1 and c_2 lie close to each other in the complex plane. Such a near degeneracy is capable of causing errors in our method as explained in §4.2. It can also cause an instability in a numerical integration (such as that of Lessen *et al.*), which might have led to errors in their results.

The general behaviour of the eigenvalues, as shown by the curves of figures 1 and 3–7, is quite similar. As $R \to 0$, the eigenvalues approach the eigenvalues of the expansion functions asymptotically. In the transition from low to high R the behaviour of the eigenvalues is extremely complicated; there are cross-overs or near cross-overs of the curves of Re (c) and Im (c). Usually it is possible to trace unambiguously the curves for the eigenvalue of a given mode through a cross-over because the eigenvalue is complex and the real parts do not cross at the same R at which the imaginary parts cross and vice versa. It should be noted that such cross-overs do not represent degeneracies, which can only occur if both the real and imaginary parts are equal.

The only case of a near degeneracy is that for modes 2 and 3 for $n = 3$ and $R \approx 125$. Calculations had to be made at intervals of $1{\cdot}0$ in R in order to elucidate the behaviour of these modes and it is still not completely clear. As shown in figures 5(*a*) and (*b*) the real parts cross while the imaginary parts repel. The approach of the imaginary parts is so close that a case could be made for a cross-over of the imaginary parts and a repulsion of the real parts. The curves of the real part of c for modes 2 and 3 would then have cusps at this point. We believe that the crossing over of the curves is much more likely than their having cusps. In either case, or even in the case of a true degeneracy, the only thing at stake is the label of a particular mode since modes 2 and 3 have the same asymptotic behaviour as $R \to \infty$.

The behaviour of the roots as $R \to \infty$ is similar for all n. The low-lying modes always group into fast and slow modes, although there is some variation with n affecting which of the low R modes becomes a fast mode and which a slow mode. However, the least-stable mode for this flow is always (R sufficiently large) a fast mode, in contrast to plane Poiseuille flow, where the least stable mode is a slow mode and the flow becomes unstable.

We have made many calculations of c for different values of n, α and R. In all cases the behaviour of the roots is similar to that shown in figures 1–7. We have found that, for $\alpha R \to \infty$, the low-lying fast modes are of the form

$$c_m = [1 - A_m(\alpha R)^{-\frac{1}{2}}] + iB_m(\alpha R)^{-\frac{1}{2}}, \tag{50}$$

† We wish to express our thanks to Dr Lessen and Dr Sadler for giving us tables of the eigenvalues which they calculated; these tables were used to prepare figure 3.

			Fast modes				Slow modes			
α	R	αR	A_1	B_1	A_2	B_2	E_1	F_1	E_2	F_2
0·5	10^4	5×10^3	6·129	3·300	3·303	6·132	3·117	1·675	5·192	1·180
1·0	5×10^3	5×10^3	6·120	3·301	3·311	6·134	3·124	1·682	5·274	1·175
2·0	$2{\cdot}5\times10^3$	5×10^3	6·083	3·305	3·342	6·142	3·135	1·702	5·473	1·247
0·1	10^5	10^4	6·124	3·309	3·304	6·129	3·072	1·692	5·445	1·125
1·0	10^4	10^4	6·124	3·301	3·308	6·133	3·143	1·721	5·581	1·149
0·1	2×10^5	2×10^4	6·095	3·292	3·314	6·141	3·035	1·515	5·798	1·074
1·0	2×10^4	2×10^4	6·126	3·301	3·306	6·133	3·158	1·752	5·844	1·169

TABLE 3. Values of the coefficients in the asymptotic formulae for the eigenvalues for $n = 2$

	Fast modes				Slow modes			
n	A_1	B_1	A_2	B_2	E_1	F_1	E_2	F_2
0	2·835	2·835	5·663	5·663	3·190	1·813	6·324	1·664
1	4·851	2·271	2·291	4·848	3·168	1·766	6·246	0·990
2	6·126	3·301	3·306	6·133	3·158	1·752	5·844	1·169
3	4·553	7·444	7·439	4·554	3·154	1·756	5·719	1·365
4	5·882	8·790	8·781	5·883	3·152	1·757	5·639	1·513
5	10·150	7·243	13·090	9·987	3·151	1·779	5·570	1·633

TABLE 4. Values of the coefficients in the asymptotic formulae for the eigenvalues, see (50) and (51)

and the low-lying slow modes are of the form

$$c_m = (E_m + iF_m)(\alpha R)^{-\frac{1}{3}}, \tag{51}$$

where A_m, B_m, E_m and F_m are real positive parameters depending on n and, in the range $0{\cdot}1 \leqslant \alpha \leqslant 10{\cdot}0$, slightly on α; m is an index labelling the modes, $m = 1$ being the least stable.

Table 3 gives values of A_m, B_m, E_m and F_m for $m = 1$ and 2, $0{\cdot}1 \leqslant \alpha \leqslant 2{\cdot}0$, $\alpha R = 5\times10^3$, 10^4 and 2×10^4 and $n = 2$. It can be seen from this table that there is a very slight variation in these coefficients with α and an even smaller variation with αR. It would appear, except perhaps for the second slow mode (coefficients E_2 and F_2), that these roots have converged to an asymptotic limit for large αR. The values of A_m, B_m, E_m and F_m for $\alpha = 1{\cdot}0$, $m = 1$ and 2, and $n = 0$–5 are given in table 4. The values for other α are only slightly different. Burridge & Drazin (1969) have published an asymptotic calculation of the stability of pipe flow which applies to the azimuthally varying as well as azimuthally symmetric modes. For $R \to 0$, they obtain the same asymptotic variation that we do. (Their eigenfunctions are, in fact, our expansion functions.) For $\alpha R \to \infty$, they obtain two sets of eigenvalues: fast modes with c varying as in (50) and slow modes with c varying as in (51). The form of this variation is in agreement with our results but the coefficients are quite different. According to Burridge & Drazin (see their equations (14) and (16)) $A_m = B_m$ and $E_m = F_m$. We find, in agreement with Pekeris, that this is true for $n = 0$, but (in complete agreement with Lessen *et al.* (1968) for $n = 1$) that these coefficients differ for $n \neq 0$.

Graebel (1970) has very recently published an analytic calculation of the stability of pipe flow for small wavenumbers. He finds, in complete *disagreement* with our results, that the flow is unstable for $n \geqslant 2$. Graebel finds very low critical Reynolds numbers, $3 \lesssim R_c^{\frac{1}{2}} \lesssim 4$ for $n = 2$, and comparatively large wavenumbers $\alpha \gtrsim 2$ (k in Graebel's notation). At such low Reynolds numbers ($R \lesssim 64$) our calculations are extremely convergent (at least 15 eigenvalues have already converged at $N = 20$) and the eigenvalues are very close to λ_k as given in (42). Since the approximations used by Graebel are only valid for small α, it may be that the appearance of instability for large α is due to the breakdown of his approximation procedure.

6. Conclusions

We have shown that expansion techniques can be applied quite straightforwardly to problems of three-dimensional disturbances. The most striking result of the calculation is that pipe flow appears to be stable to infinitesimal disturbances for all values of α, R and the azimuthal index n. In all cases the least stable mode for large Reynolds number is a fast mode ($|c| \to 1$ as $\alpha R \to \infty$) with

$$c_m = [1 - A_m(\alpha R)^{-\frac{1}{2}}] + iB_m(\alpha R)^{-\frac{1}{2}},$$

where A_m and B_m depend on the azimuthal index. This is in contrast to plane Poiseuille flow where the least stable mode is a slow mode, and the flow becomes unstable for moderate α and large but finite R.

This work was begun while the authors were on the staff of the Hudson Laboratories of Columbia University and were supported by the Office of Naval Research under Contract Nonr-266(84); it was continued and completed at the authors' present institutions. The calculations reported here were carried out at the Columbia University Computer Center, the Stevens Institute of Technology Computer Center and the Computer Education and Research Center of Pratt Institute.

REFERENCES

BURRIDGE, D. M. & DRAZIN, P. G. 1969 *Phys. Fluids* **12**, 264.

CORCOS, G. M. & SELLARS, J. R. 1959 *J. Fluid Mech.* **5**, 97.

DAVEY, A. & DRAZIN, P. G. 1969 *J. Fluid Mech.* **36**, 209.

DRYDEN, H. L. 1959 Transition from laminar to turbulent flow. In *Turbulent Flows and Heat Transfer* (ed. C. C. Lin). Princeton University Press.

FOX, J. A., LESSEN, M. & BHAT, W. V. 1968 *Phys. Fluids* **11**, 1.

GILL, A. E. 1965 *J. Fluid Mech.* **21**, 145.

GRAEBEL, W. P. 1970 *J. Fluid Mech.* **43**, 279.

GROSCH, C. E. & SALWEN, H. 1968 *J. Fluid Mech.* **34**, 177.

LESSEN, M., FOX, J. A., BHAT, W. V. & LIU, T. 1964 *Phys. Fluids* **7**, 1384.

LESSEN, M., SADLER, S. G. & LIU, T. Y. 1968 *Phys. Fluids* **11**, 1404.

PARLETT, B. N. 1967 The LU and QR algorithms. In *Mathematical Methods for Digital Computers*, vol. II (ed. A. Ralston & H. S. Wilf). John Wiley.

PEKERIS, C. L. 1948 *Proc. Natn. Acad. Sci., Wash.* **34**, 285.

PRETSCH, J. 1941 *Z. angew. Math. Mech.* **21**, 204.

RAYLEIGH, J. W. S. 1892 *Phil. Mag.* **34**, 59. (See also 1902 *Scientific Papers*, vol. III, Cambridge University Press.)

SALWEN, H. & GROSCH, C. E. 1968 *Bull. Am. Phys. Soc.* **13**, 814.

SCHENSTED, I. V. 1960 Contributions to the theory of hydrodynamic stability. Ph.D. thesis, University of Michigan.

SEXL, T. 1927 *Ann. Phys.* **83**, 835.

SYNGE, J. L. 1938 Hydrodynamic stability. *Semi-centennial Publ. Am. Math. Soc.* **2**, 227.

TATSUMI, T. 1952 *J. Phys. Soc. Japan* **7**, 489.

THOMAS, L. H. 1953 *Phys. Rev.* **91**, 780.